International Journal of Applied Earth Observations and Geoinformation 102 (2021) 102384

Contents lists available at ScienceDirect

International Journal of Applied Earth Observations and Geoinformation

journal homepage: www.elsevier.com/locate/jag

Quantitative identification of yellow rust in winter wheat with a new spectral index: Development and validation using simulated and experimental data

Yu Ren [a,b], Wenjiang Huang [a,b,c,*], Huichun Ye [a,c,*], Xianfeng Zhou [d], Huiqin Ma [a], Yingying Dong [a,b], Yue Shi [e], Yun Geng [a,b], Yanru Huang [a,b], Quanjun Jiao [a,c], Qiaoyun Xie [f]

[a] Key Laboratory of Digital Earth Science, Aerospace Information Research Institute, Chinese Academy of Sciences, Beijing 100094, China
[b] University of Chinese Academy of Sciences, Beijing 100049, China
[c] Hainan Key Laboratory of Earth Observation, Hainan Institute of Aerospace Information, Chinese Academy of Sciences, Sanya 572029, China
[d] School of Artificial Intelligence, Hangzhou Dianzi University, Hangzhou 310018, China
[e] Department of Computing and Mathematics, Manchester Metropolitan University, Manchester M1 5GD, UK
[f] Faculty of Science, University of Technology Sydney, Sydney, NSW 2138, Australia

ARTICLE INFO

Keywords:
Yellow rust
Spectral index
Hyperspectral remote sensing
Quantitative identification
PROSPECT-D model
Winter wheat

ABSTRACT

Yellow rust, caused by *Puccinia striiformis f. sp. Tritici*, is a serious disease attacking wheat (*Triticum aestivum L.*) across the globe. The occurrence of yellow rust can result in severe yield reduction and economic loss. Hyperspectral remote sensing has demonstrated potential in detecting yellow rust, with the majority of studies distinguishing qualitatively between diseased and healthy individuals or performing simple grading of disease severity. However, research on the quantification of the severity of yellow rust is limited. To fill this gap in the literature, in the current study, we constructed a new spectral index, the yellow rust optimal index (YROI), using the hyperspectral data obtained by ASD field spectrometer to quantitatively estimate yellow rust severity. The index is based on the spectral response of spores, and vegetation biophysical and biochemical parameters (VPCPs); and integrated with the PROSPECT-D model. We evaluated the new index and compared it with 11 commonly used yellow rust detection indices using experimental leaf- and canopy-scale spectral datasets. Results demonstrated the superior accuracy of YROI for both the leaf (R^2 = 0.822, RMSE = 0.070) and canopy (R^2 = 0.542, RMSE = 0.085) scales. In this research, we quantitatively analyzed the spectral response mechanism of wheat yellow rust, which provided a new idea for the quantitative identification of crop diseases. Moreover, our results can be employed as a reference and theoretical basis for the accurate and timely quantitative identification of crop diseases over the large areas in the future.

1. Introduction

As a major crop disease, yellow rust results in severe and catastrophic effects across the globe, including huge economic losses (Huang et al., 2007; Zhang et al., 2012). Yellow rust in wheat is caused by biotrophic pathogen *Puccinia striiformis f. sp. Tritici*. Leaves infected by the pathogen exhibit fungal spores that are often arranged in narrow stripes that run parallel to the leaf veins (Huang et al., 2007; Zhao et al., 2014). Mature pustules will burst and release orange-yellow masses of urediniospores. Furthermore, leaf moisture and the pigment levels within the infected tissue are altered. The infected tissue will eventually turn brown, dry out, and die (Martinez Espinoza et al., 2009). This affects the normal growth and maturity of the plant, decreasing the dry matter accumulation. The various impacts on vegetation biophysical and biochemical parameters (VPCPs) of this disease can be employed to detect the infection severity via spectroscopic techniques.

Chlorophyll is the most abundant photosynthetic pigment in plants and during plant growth; a reduction in chlorophyll content typically indicates environmental stress, disease or the aging of vegetation. Chlorophyll has been the focus of many studies (Clevers, 2012; Clevers and Gitelson, 2013; Vittorio, 2009). Changes in carotenoid (Car) content also reflect vegetation's physiological status (Young and Britton, 1990).

* Corresponding authors at: Key Laboratory of Digital Earth Science, Aerospace Information Research Institute, Chinese Academy of Sciences, Beijing 100094, China.
E-mail addresses: huangwj@aircas.ac.cn (W. Huang), yehc@aircas.ac.cn (H. Ye).

https://doi.org/10.1016/j.jag.2021.102384
Received 6 January 2021; Received in revised form 15 May 2021; Accepted 31 May 2021
Available online 11 June 2021

However, research on Car content estimation is relatively limited (Hernández-Clemente et al., 2012; Zhou et al., 2017). Leaf water content is also a strong indicator of vegetation transpiration, photosynthesis and respiration (Feret et al., 2018; Sun et al., 2019). Moreover, the leaf structure parameter (N) is crucial in determining biological species and is also an important indicator of crop physiological status, yet relevant research is lacking (Boren et al., 2019; Huang et al., 2019; Jacquemoud and Baret, 1990). Numerous studies have adopted spectroscopic approaches to estimate VPCPs based on the aforementioned parameters (Zhou et al., 2017). Radiative transfer models (RTMs) are able to clearly demonstrate the relationship between spectral reflectance and VPCPs (Zhou et al., 2019). Such models integrate spectral analysis with a deep understanding of biophysical and biochemical processes (Féret et al., 2008) in order to quickly generate large amounts of simulated spectral data for the analysis of vegetation growth states.

At present, few studies have integrated RTMs for disease detection in plants. In particular, no work has been published prior to 2018 on the effects of disease on the plant leaf structure and biochemistry based on RTM (Julien et al., 2018). Julien et al. (2018) explored the potential of combining PROSPECT-D and COSINE (PROCOSINE) to explore the biochemistry and structure responses of banana leaves infected by the fungus *Pseudocercospora fijiensis*.

Similarly, research on yellow rust in conjunction with the RTMs is particularly lacking. However, a series of studies have investigated yellow rust via hyperspectral remote sensing. For example, Huang et al. (2007) determined the photochemical reflectance index (PRI) to be highly correlated with the disease severity of wheat yellow rust. Devadas et al. (2009) employed the anthocyanin reflectance index (ARI) to differentiate wheat yellow rust from healthy wheat and wheat infected by other types of rusts. Yuan et al. (2012) adopted the spectral features of leaf data in order to differentiate wheat yellow rust and powdery mildew. Zheng et al. (2018) proposed PRI (570, 525, 705) and ARI (860, 790, 750) for the monitoring of early-mid and mid-late wheat yellow rust, respectively, with both newly proposed indices achieving promising results. Several studies also employed wavelet-based techniques for the evaluation of wheat yellow rust. In particular, Zhang et al. (2018) conducted a detailed analysis of the mother wavelet type and spectral interval effects. Shi et al. (2018) proposed a new shape-based wavelet-based rust spectral feature set (WRSFs) and determined wavelet features with the ability to trace the biophysical indicators associated with yellow rust during the disease development process.

The aforementioned studies derived spectral features suitable for yellow rust via direct spectral analysis, while the integration on plant pathology and spectroscopy remains to be implemented, and information of diseases contain in spectra is unclear. Spectral features are currently extracted by mathematical methods rather than via the underlying mechanisms of the spectral changes resulting from the disease.

In the current study, we proposed an accurate and robust index in order to identify yellow rust in winter wheat quantitatively. The index is based on the spectral response of fungal spores and VPCPs integrated with the PROSPECT-D model and the investigation of experimental data on VPCPs. The specific objectives were to: i) explore the variations in VPCPs under different disease severities; ii) investigate the spectral change patterns of wheat yellow rust under the impact of VPCPs and spore colonies (in combination with PROSPECT-D and sensitivity analysis) to determine the suitable feature bands for the index; iii) establish a new yellow rust index, YROI, for the quantitative estimation of yellow rust severity; and iv) assess the accuracy and robustness of the new index and commonly used indices in yellow rust monitoring using leaf- and canopy-scale field survey data.

2. Theory

Fig. 1 presents the pathogenesis and spectral response analysis of

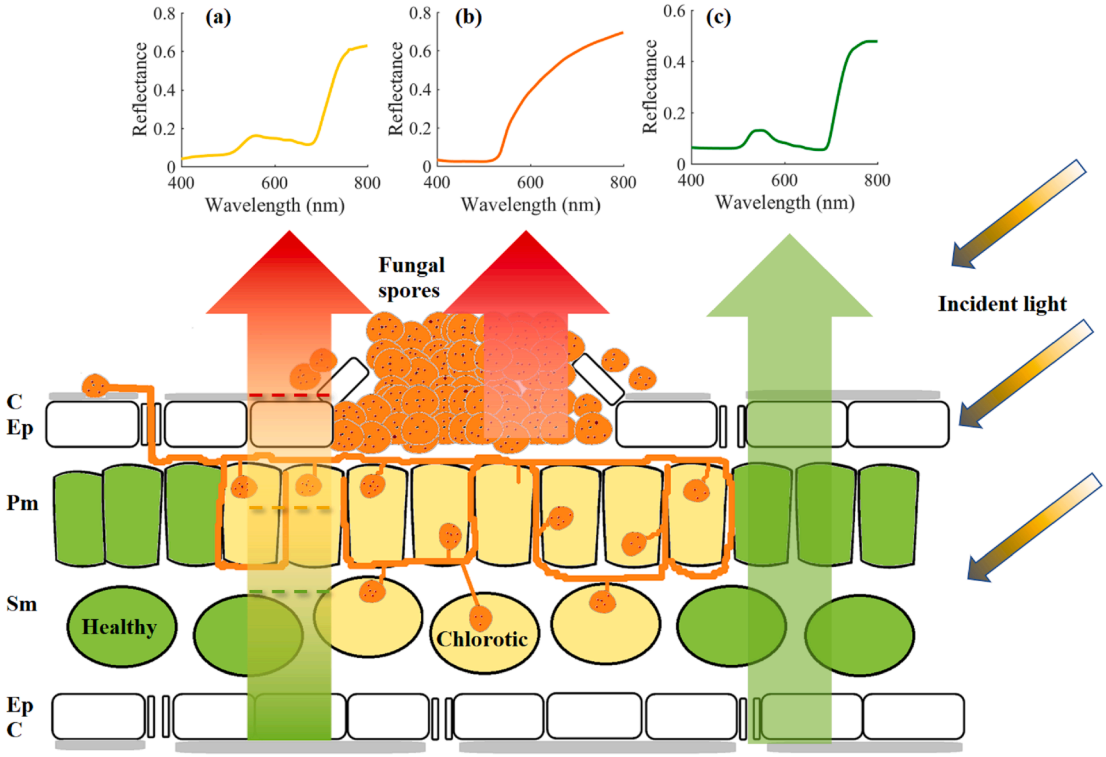

Fig. 1. Cross-sectional diagram illustrates yellow rust infesting a wheat leaf. The structure of the leaf is composed of the cuticle (C), epidermis (Ep), palisade mesophyll (Pm) and spongy mesophyll (Sm). The diagonal arrows pointing downwards indicate the incident light. The thicker, upward pointing arrows indicate the reflected signals: (a) is the mixed information of the leaf tissues infected by yellow rust and fungal spores on the leaf surface; (b) is the reflected signal of fungal spores; (c) is the spectra of a healthy leaf. The figure is modified from Bohnenkamp et al. (2019). (For interpretation of the references to color in this figure legend, the reader is referred to the web version of this article.)

wheat yellow rust. In the development of yellow rust, first, the pathogen spores grow randomly distributed pustules on the epidermis of leaves in visible to the naked eye. The colonies then grow mycelium and suckers deep below the leaf epidermal cells, and induce changes in the biophysical and biochemical content of leaves (e.g., leaf pigments, moisture, etc.). The leaves, leaf sheaths, glumes eventually exhibit slender bright yellow fungal spores and uredinium, and the leaves gradually turn yellow, with the lack of water resulting in withering. The plants subsequently become malnourished and can even die.

The reflected light carries spectral information of the leaf surface and contains the combined signal of plant tissue layers in terms of height. As shown in Fig. 1, the reflectance spectra carry information related to pigments, water content, the structure of the leaf tissue layers, and information of the thin layer of fungal spores, which has a high transmissivity. Fig. 1(c) represents a healthy leaf spectrum curve, with spectral features exhibiting a peak, valley and highly reflective feature in the green, red and near infrared bands, respectively. Fig. 1(b) depicts the fungal spore spectrum, with the reflectance increasing from 522 nm, while Fig. 1(a) is the spectrum of a leaf infected with yellow rust and thus exhibits the mixed spectrum information of the leaf tissues and fungal spores. The infected leaf spectrum demonstrates a marked change in the visible and near-infrared bands compared to the healthy spectrum.

3. Materials and methods

3.1. Experimental sites and experimental design

Two experiments were performed in this study. Experiment 1 obtained spectral and disease severity data at the leaf and canopy scales, while in Experiment 2, data on VPCPs and disease severity was collected at the leaf scale. Experiment 1 was performed at the Scientific Research and Experimental Station of the Chinese Academy of Agricultural Science (39°30′40″N, 116°36′20″E) in Langfang, Hebei province, China. Measurements were made from Feekes 6 to Feekes 10.54 (Large, 1954) during the 2017 wheat season on the wheat variety 'Mingxian 169', which is susceptible to yellow rust. On April 13, 2017, seedlings of 'Mingxian 169' were inoculated by spore inoculation using a spore water suspension. A concentration of 9 mg/100 mL spore solution was adopted to naturally generate infestation. The average nutrient status of the topsoil (0–30 cm depth) in the experiment site was as follows: organic matter content of 1.44%, total nitrogen of 0.09%, available phosphorus content of 38.2 mg/kg, and rapidly available potassium of 122.6 mg/kg. Experiment 2 was performed at the Xiaotangshan National Precision Agriculture Demonstration Research Base (40°10′36″N, 116°26′18″E), in Changping District, Beijing, China. The chlorophylls, carotenoids and leaf water contents were obtained in the laboratory at Feekes 10.51 of the 2011 growing season from the wheat variety 'Jing 9843', which was susceptible to yellow rust. The inoculation method followed that of Experiment 1. The soil type at the Xiaotangshan Research Base was silt loam soil. The average nutrient status of topsoil (0–30 cm depth) was as follows: organic matter content of 1.45%, total nitrogen content of 0.09%, alkaline hydrolysis nitrogen content of 63.6 mg/kg, available phosphorus content of 37.5 mg/kg, and available potassium content of 123.6 mg/kg.

3.2. Field measurements

3.2.1. Leaf spectra measurements

Leaf spectra were collected using the ASD FieldSpec spectrometer (Analytical Spectral Devices, Inc., Boulder, CO, USA) coupled with a Li-Cor 1800-12 integration sphere (Li-Cor, Inc., Lincoln, NE, USA). The spectrometer covers a range of 350–2500 nm with a resolution of 3 nm in the 350–1000 nm region and 10 nm in the 1000–2500 nm region, with a field of view of 25°. The sample leaves were kept in a portable refrigerator and timely transferred to the laboratory for spectral measurements. Measurements were averaged over five scans. The light source was a focused beam (Huang et al., 2014).

3.2.2. Canopy spectra measurements

Canopy spectra were also collected using the ASD FieldSpec spectrometer. The spectra were obtained under a clear sky, with minimal or no wind during 10:00–14:00 (Beijing Local Time). Canopy measurements were taken at approximately 1.3 m from the ground and averaged over ten scans. Spectra were also collected from a 0.4 m × 0.4 m white reference panel to calibrate the reflection spectra.

3.2.3. Plant measurements.

The total chlorophylls (Cab) concentration consists of chlorophyll *a* (Chla) and chlorophyll *b* (Chlb). Cab and total carotenoids (Car) concentrations were obtained using the following method. First, leaf disks of 0.25 cm^2 were collected and their fresh weight was measured. The sample leaf disks were then placed into a 95% ethanol solution in the dark at 25 °C for 48 h until they turned completely white. Following this, the samples were filtered and placed into a cuvette, where light absorption was measured at 470 nm, 649 nm and 665 nm using an UV765PC spectrophotometer (Shanghai Precision Scientific Instrument Co., LTD, Shanghai, China). Cab and Car concentrations were calculated as follows:

$$Chl_a(mg/L) = 13.95 \times A_{665} - 6.88 \times A_{649}, \quad (1)$$

$$Chl_b(mg/L) = 24.96 \times A_{649} - 7.32 \times A_{665}, \quad (2)$$

$$C_{ar}(mg/L) = (1000 \times A_{470} - 2.05 \times Chl_a - 114.8 \times Chl_b)/245, \quad (3)$$

$$C_{ab}(mg/g) = [(Chl_a + Chl_b)\left(\frac{mg}{L}\right)] \times V/[M(g) \times 1000], \quad (4)$$

$$C_{ar}(mg/g) = [Car(mg/L)] \times V/[M(g) \times 1000], \quad (5)$$

where A_x is the measured absorbance at wavelength x (nm); V is the ethanol solution volume (mL); and M is the leaf weight (g).

We also determined the leaf water content. Following the fresh weight measurements (FW (g)), the plant samples were baked in a drying oven at 105 °C for 15 min and then at 80 °C for approximately 8 h to a constant weight. The dry samples were subsequently weighed to obtain dry weight DW (g). The water content was then calculated as follows:

$$LWC(\%) = \frac{FW(g) - DW(g)}{FW(g)} \times 100\%. \quad (6)$$

3.2.4. Disease severity assessment

The leaf disease severity can be quantified using the disease ratio (DR), which is defined as the percentile portion of disease pustules coverage on the leaf. In this study, a LiDE 300 Canon scanner (Canon (China) Ltd., Beijing, China) was used to scan the disease leaves and the DR value was obtained via image processing in MATLAB (version 2016a, MathWorks, Inc., Natick, MA, USA). The data collection followed the method suggested by the National Standards for the Investigation and Forecasting of Crop Diseases (GB/T 15795-1995).

Disease index (DI) was used to investigate the canopy disease severity of wheat yellow rust. In the calculation of DI, according to the National Standards for the Investigation and Forecasting of Crop Diseases (GB/T15795-1995), the DR of leaves were divided into nine categories (1%, 10%, 20%, 30%, 45%, 60%, 80%, and 100%), where 1% represents disease level 1, 10% represents disease level 2, …, 100% represents disease level 8. And DI is calculated as follows:

$$DI = \sum(x \times f)/(n \times \sum f) \times 100 \quad (7)$$

where$x$is the disease level, n is the highest level (in this study, $n = 8$) and f is the number of leaves of each gradient.

3.3. PROSPECT-D simulation

PROSPECT (Jacquemoud and Frederic, 1990) is an improved RTM based on Allen's generalized flat-plate model. It simulates the directional-hemispheric reflectance and transmittance of vegetation leaves in the visible to short-wave infrared (400–2500 nm). In this study, we employed PROSPECT-D (Féret et al., 2017), as it demonstrated a reduced uncertainty and improved inversion accuracy of photosynthetic pigments compared to its predecessor.

In this study, five parameters were used as the input of PROSPECT-D: leaf chlorophyll content (Cab), leaf carotenoid content (Car), leaf equivalent water thickness (Cw), leaf structure parameter (N) and leaf dry matter (Cm). Each of the five parameters was sequentially set as a variable, while the remaining parameters were set as constants to observe each variable's effect on the spectra. We also set the anthocyanins and brown pigments as constants as they are not investigated here. The specific parameter settings followed Dong et al. (2019) and Huang et al. (2019) (Table 1).

The simulation data was used to perform sensitivity analysis to determine the parameters strongly sensitive to PROSPECT-D's simulated reflectance. The sensitivity analysis formula is as follows:

$$s = \frac{\sum_{i=1}^{z} \left(\boldsymbol{R}_{p}^{(i)} - \boldsymbol{R}_{p+l}^{(i)}\right)^{2}}{\boldsymbol{R}_{p}^{(1)}} \tag{8}$$

where$p$ is the input parameter of the model (N, Cab, Car, Cw, Cm, $YRspores$); l denotes the step size; $R_p^{(i)}$ is the reflectance at parameter p; $R_{p+l}^{(i)}$is the reflectance at $p + l$; and z is the number of steps ($z = 100$); i indicates the current number of parameter variations.

3.4. Spectral indices

Table 2 details the newly proposed index and 11 published spectral indices used to estimate yellow rust severity in wheat at the leaf- and canopy-scale. The published indices are the most commonly used indices for yellow rust detection. Section 4.2 describes the new index in more detail.

3.5. Analysis methods and software

Statistical significance tests were implemented in SPSS (version 20.0, IBM Corporation, New York, NY, USA), while PROSPECT-D spectral simulations were performed in ARTMO (Automated Radiative Transfer Models Operator), with a graphical user interface toolbox in MATLAB (version 2016a, MathWorks, Inc., Natick, MA, USA) (Verrelst et al., 2012). Sensitivity analysis was conducted using simulation data and the correlation coefficient (| r |) was calculated between the measured leaf spectral reflectance and the disease ratio (DR) in MATLAB. The regression model was established and validated via MATLAB. K-fold (k = 4) cross-validation was used to evaluate the performance of the spectral indices using the 2017 leaf- and canopy-scale data. All spectral indices were implemented with the same k-fold divisions. The root mean square error (RMSE) and coefficient of determination (R^2) were selected to evaluate the capability of the spectral indices in MATLAB. Details on | r |, R^2 and RMSE are available in Richter et al. (2012).

Table 1
Input parameters of PROSPECT-D for the modeling of leaf reflectance.

Parameter	Constant	Range	ΔX	n
Leaf structure parameter, N	1.41	1.0–2.0	0.01	100
Leaf chlorophyll content, Cab (μg/cm^2)	48.4	13.8–83.8	0.7	100
Leaf carotenoid content, Car (μg/cm^2)	11	3.6–13.6	0.1	100
Leaf equivalent water thickness Cw (cm)	0.00925	0.005–0.02	0.00015	100
Leaf dry matter, Cm (g/cm^2)	0.0019	0.0015–0.003	0.000015	100
Leaf anthocyanin content, Canth (μg/cm^2)	1.0	–	–	
Brown pigments, Cbp	0.0	–	–	

4. Results and discussion

4.1. Relationship between VPCPs and disease ratio (DR)

Fig. 2 presents the chlorophylls (Cab), carotenoids (Car) and leaf water contents at different DRs, which ranged from 4.024 to 1.910 mg/g, 0.512 to 0.925 mg/g, and 60.07% to 77.5%, respectively. The p-values of three variables were less than 0.001, indicating a highly significant correlation with DR.

The distribution of the Car content exhibited a downward trend with increasing leaf DR severity. Moreover, the Cab content was also observed to decrease with increasing DR. At the DR value of 0.8, the mean Cab (Car) was reduced by 37.27% (18.34%) compared to the value of the healthy sample. Water content was significantly correlated with DR (p-value < 0.001), with changes observed to be less pronounced at low DR values. The VPCPs varied as the disease progressed, and was considered as one of the fundamental causes of the spectral changes of leaves infected by yellow rust.

4.2. Spectral simulation and the establishment of the new spectral index

Fig. 3 presents all the simulation results. In the PROSPECT-D simulation, an increase in the Cab content decreased the reflectance at 450–750 nm. The key Cab absorption bands were located in the visible and red-edged bands, with the green and red-edge bands exhibiting the strongest response to a reduction in the Cab content. In particular, the reflectance of the green band increased and the red-edge band exhibited a blue-shift. The 450–550 nm wavelength range was observed to be affected by a decrease in Car content, with the most significant response near 520 nm. Car is strongly associated with crop health; when crops are stressed by pests and diseases, the Car content fluctuates. The principle leaf water absorption band is located in the infrared region between 900 and 2400 nm. Our measurements revealed the reflectance to increase as the water content decreased within this region. Variations in N resulted in spectral reflectance responses throughout the spectral range. N is related to leaf properties such as leaf cell size, shape, and distribution. In the presence of wheat yellow rust, the pathogen invades the leaf interior, causing cell death and misaligning the cell distribution. Fungal spores also attach to the leaf surface. These factors typically alter the leaf N structure. The principle dry matter absorption wavelength is located in the infrared region between 750 and 2400 nm. Spectral variations were not significant within this region.

Based on Bohnenkamp et al. (2019) and the data collected in this research, the proportion of the leaf spectrum occupied by the spore spectrum was determined as approximately 0.2, with a DR of 0.8. Therefore, when fungal spores were set as a single variable, the spore spectra were linearly mixed with the healthy leaf spectra with a proportion of 0–0.2 (the range of yellow rust (YR) spores is 0–0.2). This allowed us to investigate the effect of the spore spectra on the leaf spectra. The strongest response was observed in the spectral reflectance ranging from 530 to 800 nm. The response was most pronounced in the red band, where the reflectance gradually increased with the spore spectrum proportion increasing, and the morphology gradually flattened. In addition, a blue shift occurred in the red-edge band.

The sensitivity analysis was normalized to 0–1 to facilitate the co-presentation with the correlation analysis results (Fig. 4). Correlation analysis was performed with the measured leaf spectral reflectance and DR to determine the | r | of the spectral bands. In the research, we only considered the visible and near-infrared bands (400–800 nm).

The sensitivity of Cab was observed to be relatively high compared to the other factors (Fig. 4). The two local maxima in the sensitivity

Table 2
Proposed and published indices used to investigate yellow rust severity in this study.

Index	Related To	Formula	Reference
Normalized Difference Vegetation Index (NDVI)	Vegetation coverage	$(R_{800} - R_{670})/(R_{800} + R_{670})$	Rouse et al. (1974)
Modified Simple Ratio Index (MSR)	Leaf area	$(\frac{R_{800}}{R_{670}} - 1)/(\frac{R_{800}}{R_{670}} + 1)^{1/2}$	Chen (1996)
Structure Insensitive Pigment Index (SIPI)	Pigment content	$(R_{800} - R_{445})/(R_{800} - R_{680})$	Penuelas et al. (1995)
MERIS Terrestrial Chlorophyll Index (MTCI)	Chlorophyll absorption	$(R_{750} - R_{710})/(R_{710} - R_{680})$	Dash and Curran (2004)
Photochemical Reflectance Index (PRI)	Photosynthetic radiation	$(R_{531} - R_{570})/(R_{531} + R_{570})$	Gamon et al. (1992)
Plant Senescence Reflectance Index (PSRI)	Pigment senescence	$(R_{680} - R_{500})/R_{750}$	Merzlyak et al. (2010)
Triangular Vegetation Index (TVI)	Plant status	$\frac{120(R_{750} - R_{550}) - 200(R_{670} - R_{550})}{2}$	Broge and Leblanc (2001)
Modified Chlorophyll Absorption Reflectance Index (MCARI)	Chlorophyll absorption	$((R_{701} - R_{671}) - 0.2(R_{701} - R_{549}))/(R_{701}/R_{671})$	Daughtry et al. (2000)
Physiological Reflectance Index (PhRI)	Light use efficiency	$(R_{550} - R_{531})/(R_{550} + R_{531})$	Gamon et al. (1992)
Anthocyanin Reflectance Index (ARI)	Anthocyanin content	$(R_{550})^{-1} - (R_{700})^{-1}$	Gitelson et al. (2010)
Ratio Vegetation Structure Index (RVSI)	Internal structure parameter	$((R_{712} + R_{752})/2) - R_{732}$	Merton and Huntington (1999)
Yellow Rust Optimal Index (YROI)	Yellow rust	$(R_{611} - R_{452})/R_{550}$	This study

R_λ is the reflectance value at wavelength λ.

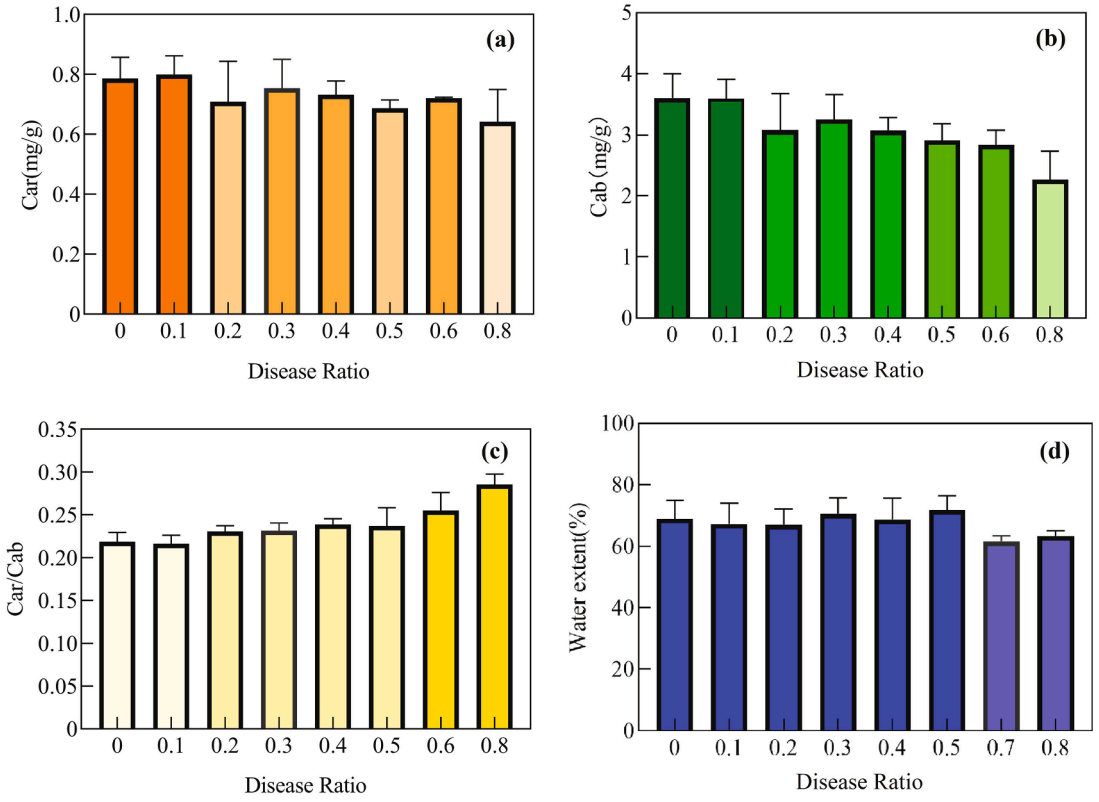

Fig. 2. Effect of an increasing disease ratio (DR) on (a) carotenoid (Car) content; (b) chlorophyll (Cab) content; (c) ratio of Car to Cab content (Car/Cab); and (d) water content.

analysis curve are located at 603 nm and 698 nm, respectively. The high sensitivity of YR spores was dominant in the red band, with the maximum at 682 nm. The sensitivity of the N structure was moderate, yet still contributed to the overall result. A small peak for Car was observed between 500 and 550 nm.

The correlation analysis between the leaf spectral bands and DR revealed a high correlation ($|r| > 0.6$) within 540 to 712 nm, with the maximum correlation at 611 nm ($|r| = 0.7862$). The sensitivity analysis results indicated the high correlation to be attributed to the combined contribution of Cab, spores, and N structure.

The sensitivity of each factor was relatively low within the 400–500 nm range. This region also corresponded to low correlation $|r|$ values, with the minimum observed at 452 nm. This wavelength is poorly correlated with the disease and relatively more correlated with the information of the crop, and can thus be used as a reference band.

The yellow rust optimal index (YROI) was constructed using 611 nm, 452 nm and 550 nm based on the analysis above. The 611 nm and 452 nm bands are located on either side of the green band of the vegetation spectral curve. As the peak of the green band, 550 nm band can reflects the physiological information of the crop. The selected wavelengths in the yellow (611 nm), green (550 nm) and blue (452 nm) bands are able to reflect the crop color and the morphology of the green peak of the

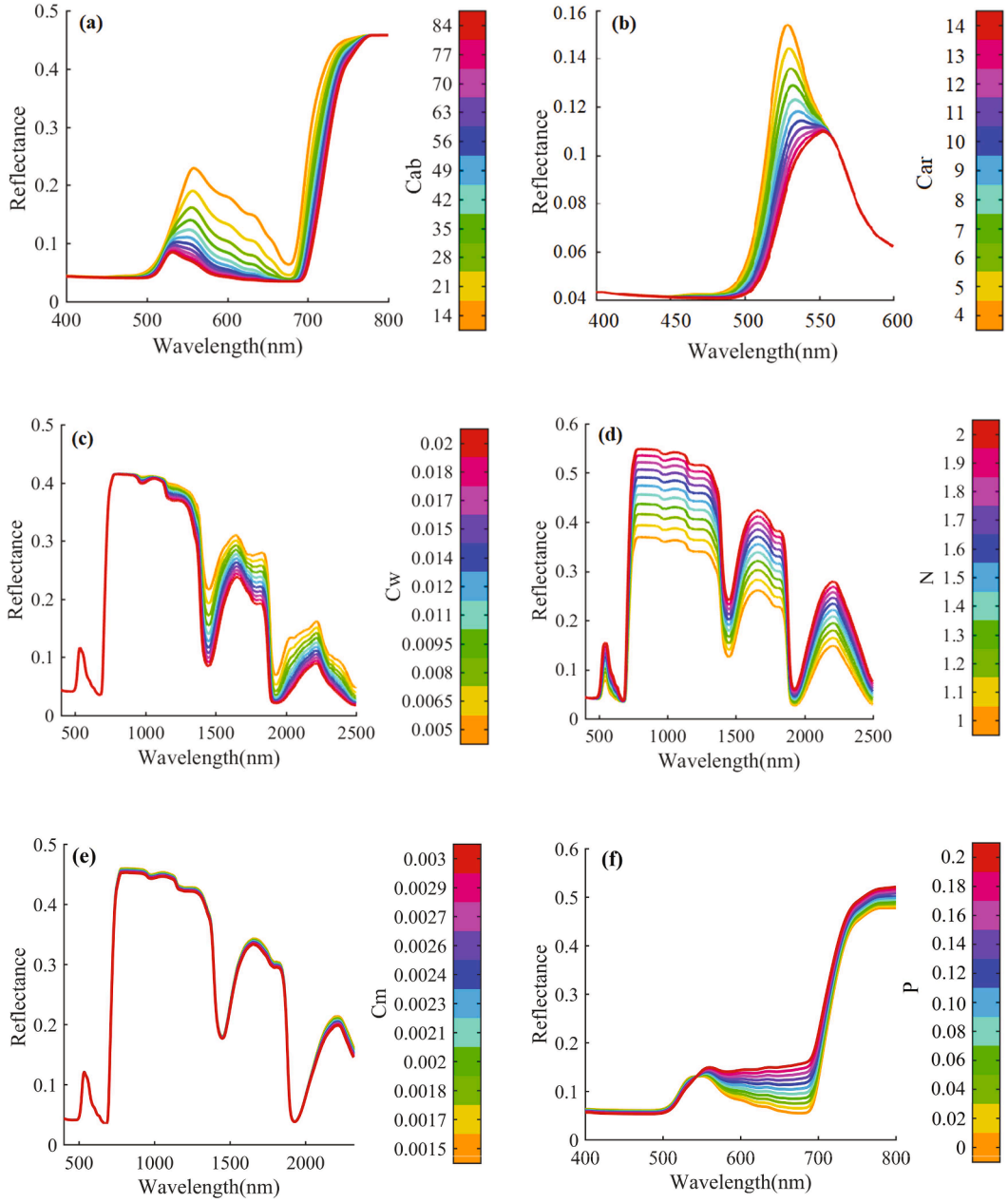

Fig. 3. Variations in the reflectance of simulated spectra with different contents of biophysical and biochemical parameters by PROSPECT-D model, and simulated spectra with different proportions of fungal spores: (a) leaf chlorophyll content, Cab (μg/cm^2); (b) leaf carotenoid content, Car (μg/cm^2); (c) leaf equivalent water thickness, Cw (cm); (d) leaf structure parameter, N; (e) leaf dry matter, Cm (g/cm^2); (f) proportion of spore spectra to mixed spectra, P.

vegetation spectral curve. Therefore, the yellow rust optimal index (YROI) was constructed using 611 nm, 452 nm and 550 nm and was determined as $(R_{611} - R_{452})/R_{550}$. The newly proposed index is able to simultaneously remove additional information related to the vegetation and highlight the yellow rust infestation information.

4.3. Disease ratio (DR) assessment with spectral indices at the leaf scale

We compared the proposed index with 11 vegetation indices commonly used in the literatures for yellow rust. Fig. 5 presents the results of the 4-fold cross-validation. The newly proposed index, YROI, demonstrated strong linearity and the highest correlation ($R^2 = 0.822$, RMSE = 0.070). The fitted line of the scatterplot was close to the 1:1 line (Slope = 0.834). The photochemical reflectance index, PRI, yielded the best estimation among the published indices ($R^2 = 0.704$, RMSE = 0.084), with a strong ability to reflect the physiological activity of the leaves. Huang et al. (2007) demonstrated that the PRI was able to quantify the disease level of wheat yellow rust. The PSRI also yielded satisfactory results, with a R^2 of 0.685 (RMSE = 0.085). The R^2 of two chlorophyll indices, SIPI and MTCI, were above 0.6, while the other chlorophyll index, MCARI, only achieved an accuracy of 0.509. As the disease progresses, a reduction in chlorophyll content is just one of the numerous symptoms of yellow rust. Thus, although monitoring chlorophyll content was able to reflect crop health conditions to some extent, it did not directly reflect the DR of wheat leaves. This can explain why the chlorophyll index was able to just partially reflect yellow rust severity. Despite ranking relatively low in the selected indices, the R^2 of PhRI, NDVI, and MSR were still close to 0.6, indicating a correlation with yellow rust severity. TVI, ARI and RVSI exhibited poor prediction ability, implying their possible insensitivity to the leaf DR of yellow rust.

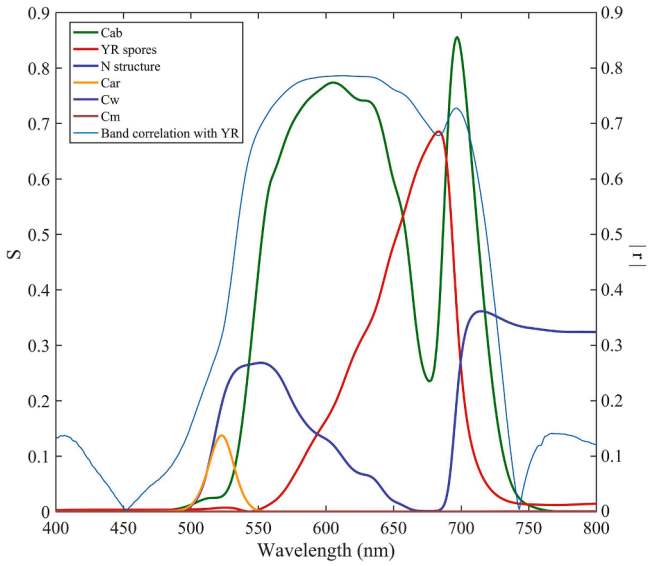

Fig. 4. Sensitivity analysis results of the parameters (Cab, yellow rust (YR) spores, N structure, Car, Cw and Cm) and the corresponding correlation analysis result between the measured leaf spectral reflectance and disease ratio (DR). The left and right y-axes represent the sensitivity (S) (which is normalized to 0–1) and the absolute value of the correlation coefficient (| r |), respectively.

4.4. Disease index (DI) assessment with spectral indices at the canopy scale

The wheat canopy spectral data and disease index (DI) were used to evaluate the feasibility of the new indices at the canopy scale. Fig. 6 presents the 4-fold cross-validation results. YROI exhibited the highest accuracy (R^2 = 0.542; RMSE = 0.085) out of all indices. Furthermore, the stability and robustness of the newly proposed index surpassed those of the other indices. PRI and PSRI also yielded satisfactory results at the canopy scale. PRI exhibited the optimal estimation performance in the published indices, with a R^2 and RMSE of 0.514 and 0.086, respectively. PRI thus achieved favorable results in both the leaf and canopy scales. This is consistent with Huang et al. (2007). Although lower than that of PRI, the accuracy of PSRI was relatively high in the leaf data, and satisfactory results were also obtained in the canopy data. As an indicator of plant senescence, PSRI can also effectively reflect the physiological status of vegetation and is thus suitable for estimating the disease level of yellow rust at the leaf and canopy scale. ARI exhibited a better performance in the canopy measurements compared to the leaf scale, indicating its suitability for canopy-scale disease severity estimations of yellow rust. PhRI was centrally ranked (fifth place) in the canopy-scale cross-validation, with a R^2 of 0.358 and a RMSE of 0.084. This index thus also demonstrated an ability to detect yellow rust severity both at leaf- and canopy-scale. The three chlorophyll indices performed relatively poor in the cross-validation of the canopy data compared to the leaf scale. SIPI (R^2 = 0.354; RMSE = 0.083), MTCI (R^2 = 0.251; RMSE = 0.077) and MCARI (R^2 = 0.033; RMSE = 0.046) ranked sixth, ninth and eleventh place, respectively. This suggests the better suitability of SIPI and MTCI for leaf-scale yellow rust detection. However, the performance of MCARI was poor at both the leaf- and canopy-scale and it was thus not considered as a suitable index for the disease severity of yellow rust. MSR and NDVI ranked seventh (R^2 = 0.327; RMSE = 0.082) and eighth (R^2 = 0.287; RMSE = 0.079) respectively. Although they are able to reflect the severity of yellow rust to some extent, they are not optimal for this application. TVI and RVSI ranked tenth (R^2 = 0.191; RMSE = 0.072) and twelfth. (R^2 = 0.020; RMSE = 0.034), with a similar performance at the leaf scale. This indicates that they are not suitable for disease severity estimation of yellow rust.

The selected published indices are the most commonly used indices for the detection of yellow rust. Therefore, although they are not as accurate and robust as the new index, the majority is capable of estimating the severity of yellow rust. Numerous studies have qualitatively identified yellow rust in winter wheat using these published indices (Jiang et al., 2007; Zheng et al., 2018). However, research on the quantitative inversion of yellow rust severity is limited. Among the commonly used indices, only PRI and PSRI have yielded satisfactory results in this research. Furthermore, the experiments at the leaf- and canopy-scale in the current study reveal the ability of our newly proposed index to outperform the published indices.

4.5. Future work

This research focuses on the spectral response to yellow rust in wheat from a microscopic perspective. By performing quantitative studies on the spectral response of VPCPs and yellow rust spores, the sensitive bands of wheat yellow rust were found and a spectral index sensitive to yellow rust was developed. The new index was validated using leaf and canopy scale data.

Future research will test the results of current study on hyperspectral and multispectral imagery, while examining the effect of the atmosphere on the new index for quantitative identification of yellow rust. In the following, we will discuss the possibility of the new index to be applied on images and discuss how scale effects and atmospheric factors may affect the application.

Current remote sensing imagery can meet the band settings of the new index. Unmanned aerial vehicle (UAV) or satellite hyperspectral imagery can be of a high spectral resolutions. Previous research has been conducted on yellow rust using UAVs (Guo et al., 2021; Su et al., 2018). Such imagery can be used to calculate the hyperspectral index YROI. For example, the S185 imaging spectrometer (Cubert GmbH, Ulm, Baden-Württemberg, Germany) which can be equipped on a UAV, is capable of acquiring hyperspectral data in the spectral range of 450–950 nm, with a high spatial resolution of 125 effective bands at 4 nm sampling intervals (Guo et al., 2021). The PRISMA Earth observation satellite, successfully launched in 2019, covers the spectral range from the visible to the shortwave infrared with a spectral resolution of 12 nm (Loizzo et al., 2018). The new proposed index can be determined from this satellite hyperspectral imagery as the three bands of the newly proposed index YROI are located in the blue, green, and yellow bands. Multispectral images typically do not have the yellow band, thus migrating the YROI to multispectral imagery can be hard. However, Worldview-2 satellite images meet the band composition requirements of the new index with blue (450–510 nm), green (510–580 nm), and yellow (585–625 nm) bands (Robinson et al., 2016).

The aforementioned sensors are able to meet the requirements in the spectral dimension. However, the issue of scale effect in spatial dimension must be considered(Hua and Li, 2009). Our research is a mechanistic study of the spectral response of yellow rust at the leaf and canopy scales based on ground-based hyperspectral data. However, the information contained in the image pixels at different scales (different spatial resolutions) is distinct from the ground-based data in this research. For example, the S185 imaging spectrometer is able to acquire images with a spatial resolution of approximately 1.2 cm when the UAV is at altitude of 50 m, and 0.8 cm at 30 m. Therefore, the new index proposed in this paper based on leaf-scale spectra can be comparable to high-resolution UAV images. However, since the mixed pixels in the images may also contain information on soil and shadow, further tests are required. PRISMA has a 30 m spatial resolution in the multispectral band and a 5 m spatial resolution in the panchromatic band. Unlike the leaf and canopy scale information obtained in this study, each PRISMA pixel provides information of the field. Therefore, the applicability of YROI in PRISMA requires further validation. Worldview-2 imagery as an example, it has a spatial resolution of 1.8 m in multispectral bands and a spatial resolution of 0.46 m in the panchromatic band. The information obtained at this resolution can be regarded as canopy-scale information.

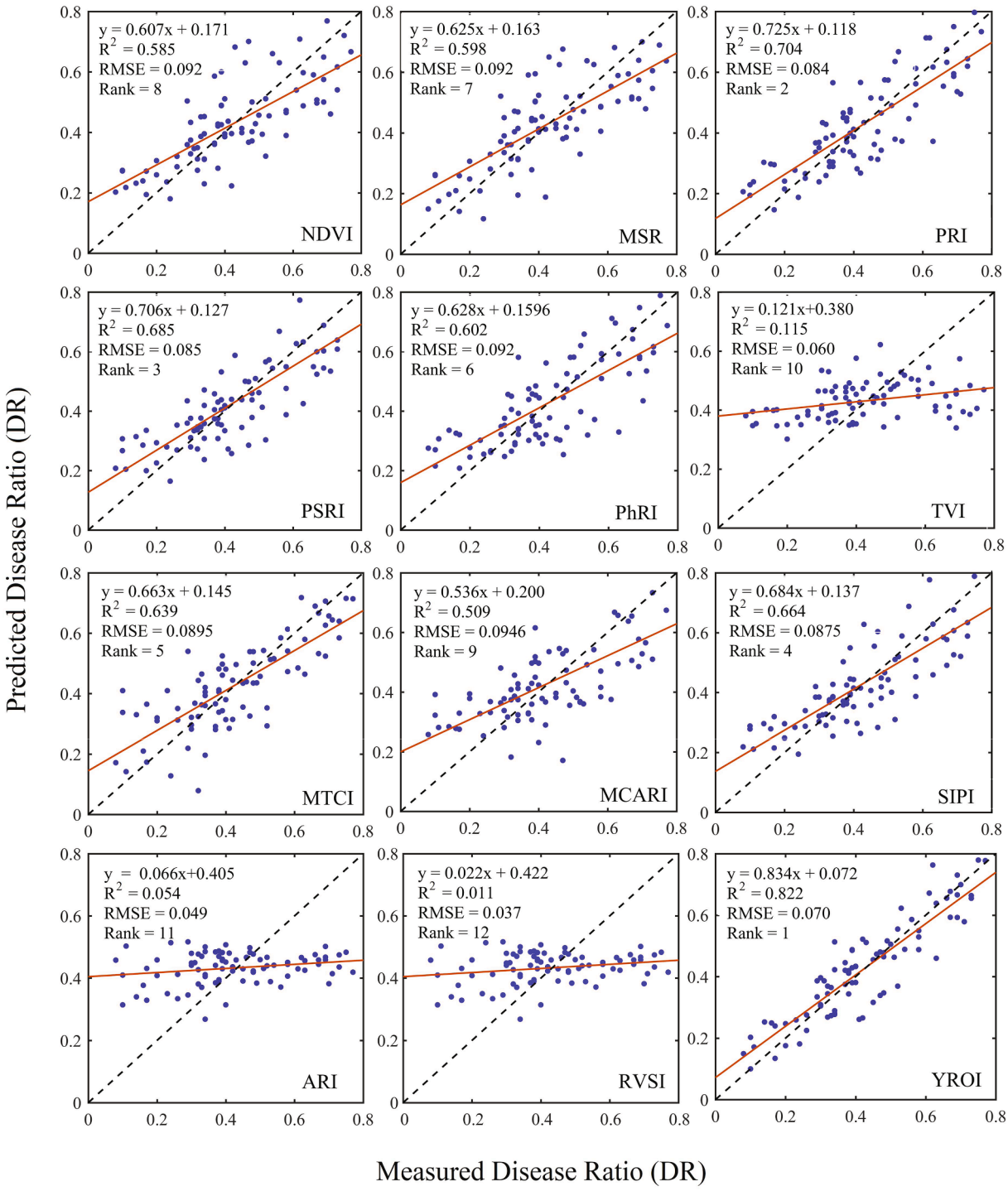

Fig. 5. Scatterplots of the measured disease ratio (DR) versus predicted DR for vegetation indices with leaf-scale data (n = 84). The 1:1 line is shown as the dashed line. The vegetation index is indicated in the lower part of each graphic. A description of each vegetation index is given in Table 2.

YROI is able to obtain good quantitative identification at the canopy scale, and thus has the potential to migrate to Worldview-2 images. However, the images also contain information on soil, shading, etc. Therefore, further discussion is required to determine a solution for this.

UAV images are essentially not affected by the atmosphere due to the low flight altitude, yet water vapor effects are prominent. However, YROI does not use absorption bands of water vapor and thus influence of the atmosphere and water vapor can be ignored. In contrast, application of YROI in satellite imagery is affected by the atmosphere. The top of atmosphere reflectance contains atmospheric path radiation, which interferes with the useful information of surface reflectance (SR) (Gao et al., 2009). There are currently satellite SR products that have eliminated atmospheric effects. However, currently, Worldview-2 does not have its own SR products, while atmospheric effects can be eliminated via atmospheric correction. Although the visible band is located in the atmospheric window, the shorter wavelengths in the visible band are more susceptible to the effect of atmospheric scattering, weakening the electromagnetic wave energy entering the blue channel. Therefore, the weakened reflectance information of the blue band may influence YORI calculation.

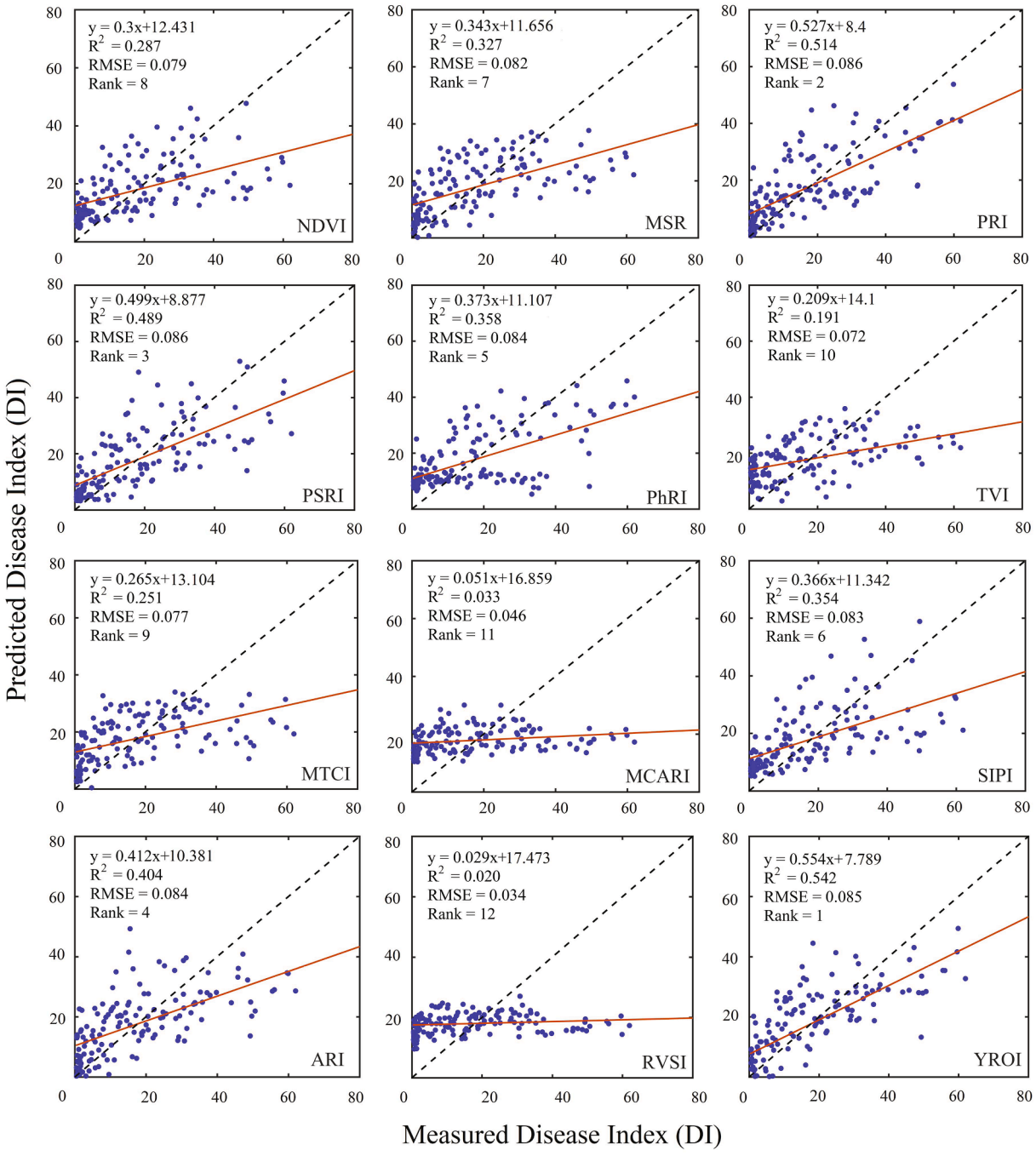

Fig. 6. Scatterplots of measured disease index (DI) versus predicted DI for vegetation indices with canopy-scale data (n = 143). The 1:1 line is shown as the dashed line. The vegetation index is indicated in the lower part of each graphic. A description of each vegetation index is given in Table 2.

5. Conclusion

In the current study, we analyzed the pathogenesis of wheat yellow rust and investigated the variations in VPCPs by increasing disease severity. PROSPECT-D was used to simulate and analyze the effects of VPCPs on the spectra, and the effect of spore colonies on the spectra was also considered using linear mixing. Sensitivity and correlation analysis were performed to obtain the sensitive bands for the construction of YROI. We tested the newly established index's accuracy and robustness by comparing it with current commonly used indices using leaf- and canopy-scale spectral data. YROI surpassed the other indices in the leaf- and canopy-scale cross-validation. The accurate and robust YROI for quantitatively determining the disease severity of yellow rust provides a basis for the timely and accurate judgment and treatment of yellow rust in precision agricultural applications.

Although the index yielded optimal results in ground-based hyperspectral data, we did not validate it using imagery. YROI should be tested and improved using multispectral and hyperspectral imagery based on the numerous sources of uncertainty of such imagery (e.g., scale effect and atmosphere influence). This will provide a reference for the accurate and timely quantitative identification of crop diseases using remote sensing imagery over large areas.

CRediT authorship contribution statement

Yu Ren: Conceptualization, Methodology, Writing - original draft, Software. **Wenjiang Huang:** Methodology, Supervision. **Huichun Ye:** Writing - review & editing, Methodology. **Xianfeng Zhou:** Writing - review & editing. **Huiqin Ma:** Software, Writing - review & editing. **Yingying Dong:** Project administration, Supervision. **Yue Shi:** Resources. **Yun Geng:** Formal analysis. **Yanru Huang:** Investigation. **Quanjun Jiao:** Data curation. **Qiaoyun Xie:** Validation.

Declaration of Competing Interest

The authors declare that they have no known competing financial interests or personal relationships that could have appeared to influence the work reported in this paper.

Acknowledgments

The research was funded by the National Key Research and Development Program of China (2017YFE0122400), Funding from CAS (183611KYSB20200080), National Natural Science Foundation of China (42071320, 42071423, 41901369), National Special Support Program for High-level Personnel Recruitment (Wenjiang Huang), Youth Innovation Promotion Association CAS (Huichun Ye). The author would like to thank the reviewers who provided comments and suggestions on the paper, and the people who collected the experimental data during the fieldwork.

References

Bohnenkamp, D., Kuska, M.T., Mahlein, A.K., Behmann, J., 2019. Hyperspectral signal decomposition and symptom detection of wheat rust disease at the leaf scale using pure fungal spore spectra as reference. Plant. Pathol. 68.

Boren, E.J., Boschetti, L., Dan, M.J., 2019. Characterizing the variability of the structure parameter in the PROSPECT leaf optical properties model. Remote Sens. 11, 1236.

Broge, N.H., Leblanc, E., 2001. Comparing prediction power and stability of broadband and hyperspectral vegetation indices for estimation of green leaf area index and canopy chlorophyll density. Remote Sens. Environ. 76, 156–172.

Chen, J., 1996. Evaluation of vegetation indices and a modified simple ratio for boreal applications. Can. J. Remote Sens. 22.

Clevers, J.G.P.W., 2012. Using hyperspectral remote sensing data for retrieving canopy chlorophyll and nitrogen content. IEEE J. Sel. Top. Appl. Earth Obs. Remote Sens. 5, 574–583.

Clevers, J.G.P.W., Gitelson, A.A., 2013. Remote estimation of crop and grass chlorophyll and nitrogen content using red-edge bands on Sentinel-2 and -3. Int. J. Appl. Earth Obs. Geoinf. 23, 344–351.

Dash, J., Curran, P.J., 2004. The MERIS terrestrial chlorophyll index. Int. J. Remote Sens. 25 (23), 5403–5413. https://doi.org/10.1080/0143116042000274015.

Daughtry, C.S.T., Walthall, C.L., Kim, M.S., Colstoun, E.B.D., Iii, M.M., 2000. Estimating corn leaf chlorophyll concentration from leaf and canopy reflectance. Remote Sens. Environ. 74, 229–239.

Devadas, R., Lamb, D.W., Simpfendorfer, S., Backhouse, D., 2009. Evaluating ten spectral vegetation indices for identifying rust infection in individual wheat leaves. Precis. Agric. 10, 459–470.

Dong, T., Shang, J., Chen, J.M., Liu, J., Zhou, G., 2019. Assessment of portable chlorophyll meters for measuring crop leaf chlorophyll concentration. Remote Sens. 11, 2706.

Féret, J.-B., Francois, C., Asner, G., Gitelson, A., Martin, R., Bidel, L., Ustin, S., le Maire, G., Jacquemoud, S., 2008. PROSPECT-4 and 5: Advances in the leaf optical properties model separating photosynthetic pigments. Remote Sens. Environ. 112, 3030–3043.

Féret, J.B., Gitelson, A.A., Noble, S.D., Jacquemoud, S., 2017. PROSPECT-D: towards modeling leaf optical properties through a complete lifecycle. Remote Sens. Environ. 193, 204–215.

Féret, J.-B., le Maire, G., Jay, S., Berveiller, D., Bendoula, R., Hmimina, G., Cheraiet, A., Oliveira, J.C., Ponzoni, F.J., Solanki, T., de Boissieu, F., Chave, J., Nouvellon, Y., Porcar-Castell, A., Proisy, C., Soudani, K., Gastellu-Etchegorry, J.-P., Lefèvre-Fonollosa, M.-J., 2018. Estimating leaf mass per area and equivalent water thickness based on leaf optical properties: Potential and limitations of physical modeling and machine learning. Remote Sens. Environ. 231, 110959. https://doi.org/10.1016/j.rse.2018.11.002.

Gamon, J.A., Pe?Uelas, J., Field, C.B., 1992. A narrow-waveband spectral index that tracks diurnal changes in photosynthetic efficiency. Remote Sens. Environ. 41, 35-44.

Gao, B.C., Montes, M.J., Davis, C.O., Goetz, A., 2009. Atmospheric correction algorithms for hyperspectral remote sensing data of land and ocean. Remote Sens. Environ. 113, S17–S24.

Gitelson, A.A., Merzlyak, M.N., Chivkunova, O.B., 2010. Optical properties and nondestructive estimation of anthocyanin content in plant leaves. Photochem. Photobiol. 74, 38–45.

Guo, A., Huang, W., Dong, Y., Ye, H., Geng, Y., 2021. Wheat yellow rust detection using UAV-based hyperspectral technology. Remote Sens. 13, 123.

Hernández-Clemente, R., Navarro-Cerrillo, R.M., Zarco-Tejada, P.J., 2012. Carotenoid content estimation in a heterogeneous conifer forest using narrow-band indices and PROSPECT+DART simulations. Remote Sens. Environ. 127, 298–315.

Hua, W., Li, Z.L., 2009. Scale issues in remote sensing: a review on analysis, processing and modeling. Sensors 9, 1768–1793.

Huang, S., Chen, S., Wang, D., Zhou, C., Van, d.M.F., Zhang, Y., 2019. Hydrocarbon micro-seepage detection from airborne hyper-spectral images by plant stress spectra based on the PROSPECT model. Int. J. Appl. Earth Obs. Geoinf. 74, 180–190.

Huang, W., Guan, Q., Luo, J., Zhang, J., Zhao, J., Liang, D., Huang, L., Zhang, D., 2014. New optimized spectral indices for identifying and monitoring winter wheat diseases. selected topics in applied earth observations and remote sensing. IEEE J. 7, 2516–2524.

Huang, W., Lamb, D.W., Niu, Z., Zhang, Y., Liu, L., Wang, J., 2007. Identification of yellow rust in wheat using in-situ spectral reflectance measurements and airborne hyperspectral imaging. Precis. Agric. 8, 187–197.

Jacquemoud, S., Baret, F., 1990. PROSPECT: A model of leaf optical properties spectra. Remote Sens. Environ 34, 75–91.

Jacquemoud, S., Frederic, B., 1990. PROSPECT: a model of leaf optical properties spectra. Remote Sens. Environ. 34, 75–91.

Jiang, J., Chen, Y., Gong, A., Li, J., 2007. Study on inversion models for the severity of winter wheat stripe rust using hyperspectral remote sensing. IEEE Int. Geosci. Remote Sens. Symposium.

Julien, Morel, Sylvain, Jay, Jean-Baptiste, Féret, Adel, Bakache, Ryad, Bendoula, 2018. Exploring the potential of PROCOSINE and close-range hyperspectral imaging to study the effects of fungal diseases on leaf physiology. Sci. Rep.

Loizzo, R., Guarini, R., Longo, F., Scopa, T., Varacalli, G., 2018. Prisma: The Italian Hyperspectral Mission, IGARSS 2018 - 2018 IEEE International Geoscience and Remote Sensing Symposium.

Martinez Espinoza, A., Youmans, J., Buck, J., 2009. Stripe Rust (Yellow Rust) of Wheat.

Merton, R., Huntington, J., 1999. Early simulation results of the ARIES-1 satellite sensor for multi-temporal vegetation research derived from AVIRIS.

Merzlyak, M.N., Chivkunova, O.B., Gitelson, A.A., Rakitin, V.Y., 2010. Non-destructive optical detection of pigment changes during leaf senescence and fruit ripening. Physiol. Plant. 106, 135–141.

Penuelas, J., Baret, F., Filella, I., 1995. Semi-empirical indices to assess carotenoids/chlorophyll-a ratio from leaf spectral reflectance. Photosynthetica 31, 221–230.

Richter, K., Atzberger, C., Hank, T.B., Mauser, W., 2012. Derivation of biophysical variables from Earth observation data: validation and statistical measures. J. Appl. Remote Sens. 6, 3557.

Robinson, T.P., Wardell-Johnson, G.W., Pracilio, G., Brown, C., Klinken, R., 2016. Testing the discrimination and detection limits of WorldView-2 imagery on a challenging invasive plant target. Int. J. Appl. Earth Obs. Geoinf. 44, 23–30.

Rouse, J., Haas, R., Schell, J., Deering, D., 1974. Monitoring vegetation systems in the great plains with ERTS. NASA Special Publication 1.

Shi, Y., Huang, W., Pablo, G.M., Belinda, L., Dong, Y., Zheng, Q., Ma, H., Liu, L., 2018. Wavelet-based rust spectral feature set (WRSFs): A novel spectral feature set based on continuous wavelet transformation for tracking progressive host-pathogen interaction of yellow rust on wheat. Remote Sens. 10, 525.

Su, J., Liu, C., Coombes, M., Hu, X., Chen, W.H., 2018. Wheat yellow rust monitoring by learning from multispectral UAV aerial imagery. Comput. Electron. Agric. 155, 157–166.

Sun, J., Shi, S., Yang, J., Gong, W., Qiu, F., Wang, L., Du, L., Chen, B., 2019. Wavelength selection of the multispectral lidar system for estimating leaf chlorophyll and water contents through the PROSPECT model. Agricultural & Forest Meteorology s 266–267, 43–52.

Verrelst, J., Romijn, E., Kooistra, L., 2012. Mapping vegetation density in a heterogeneous river floodplain ecosystem using pointable CHRIS/PROBA data. Remote Sens. 4, 2866–2889.

Vittorio, A.V.D., 2009. Enhancing a leaf radiative transfer model to estimate concentrations and in vivo specific absorption coefficients of total carotenoids and chlorophylls a and b from single-needle reflectance and transmittance. Remote Sens. Environ. 113, 1948–1966.

Young, A., Britton, G., 1990. Carotenoids and stress. Carotenoids and Stress 87–112.

Yuan, L., Zhang, J., Zhao, J., Du, S., Wang, J., 2012. Discrimination of yellow rust and powdery mildew in wheat at leaf level using spectral signatures. First International Conference on Agro-geoinformatics.

Zhang, J., Pu, R., Huang, W., Lin, Y., Luo, J., Wang, J., 2012. Using in-situ hyperspectral data for detecting and discriminating yellow rust disease from nutrient stresses. Field Crops Res. 134, 165–174.

Zhang, J., Wang, B., Zhang, X., Liu, P., Huang, W., 2018. Impact of spectral interval on wavelet features for detecting wheat yellow rust with hyperspectral data. Int. J. Agric. Biol. Eng. 11, 138–144.
Zhao, J., Huang, L., Huang, W., Zhang, D., Yuan, L., Zhang, J., Liang, D., 2014. Hyperspectral measurements of severity of stripe rust on individual wheat leaves. Eur. J. Plant Pathol. 139, 407–417.
Zheng, Q., Huang, W., Cui, X., Dong, Y., Shi, Y., Ma, H., Liu, L., 2018. Identification of wheat yellow rust using optimal three-band spectral indices in different growth stages. Sensors 19 (1), 35.
Zhou, X., Huang, W., Kong, W., Ye, H., Dong, Y., Casa, R., 2017. Assessment of leaf carotenoids content with a new carotenoid index: Development and validation on experimental and model data. Int. J. Appl. Earth Obs. Geoinf. 57, 24–35.
Zhou, X., Huang, W., Zhang, J., Kong, W., Casa, R., Huang, Y., 2019. A novel combined spectral index for estimating the ratio of carotenoid to chlorophyll content to monitor crop physiological and phenological status. Int. J. Appl. Earth Obs. Geoinf. 76, 128–142.